SPIE Conference on Radiation Detectors: Systems and Applications XVI **DOE/NV/25946--2432**
San Diego, CA; August 9-13, 2015

Linearity response of Ca^{2+}-doped $CeBr_3$ as a function of gamma ray energy

Paul Guss*[a], Michael E. Foster,[b] Bryan M. Wong,[b] F. Patrick Doty,[b] Kanai Shah,[c] Michael R. Squillante,[c] Urmila Shirwadkar,[c] Rastgo Hawrami,[c] Josh Tower,[c] Thomas Stampahar,[a] and Sanjoy Mukhopadhyay[d]

[a]National Security Technologies, LLC, Remote Sensing Laboratory–Nellis, P.O. Box 98521, M/S RSL-09, Las Vegas, NV 89193-8521, USA; [b]Sandia National Laboratories, California, Materials Chemistry Department, P.O. Box 969, Livermore, CA 94551-0969, USA; [c]Radiation Monitoring Devices, Inc., 44 Hunt Street, Watertown, MA 02472, USA; [d]National Security Technologies, LLC, Remote Sensing Laboratory–Andrews, Building 1783, Arnold Avenue, Andrews AFB, MD 20762, USA

ABSTRACT

An aliovalently calcium-doped cerium tribromide (CeBr3:Ca2+) crystal was prepared with a gamma-energy resolution (FWHM) of 3.2% at the ^{137}Cs 662 keV gamma energy. We completed a crystal assessment and calculated the predictive performance and physical characteristics using density functional theory (DFT) formalism. Detector performance, characteristics, calcium doping concentration, and crystal strength are reported. The structural, electronic, and optical properties of $CeBr_3$ crystals were investigated using the DFT within generalized gradient approximation. Specifically, we see excellent linearity of photons per unit energy with the aliovalent $CeBr_3$:Ca^{2+} crystal. Proportionality of light yield is one area of performance in which Ce-doped and Ce-based lanthanide halides excel. Maintaining proportionality is the key to producing a strong, high-performance scintillator. Relative light yield proportionality was measured for both doped and undoped samples of $CeBr_3$ to ensure no loss in performance was incurred by doping. The light output and proportionality for doped $CeBr_3$, however, appears to be similar to that of undoped $CeBr_3$. The new crystal was subjected to additional testing and evaluation, including a benchmark spectroscopy assessment. Results, which present energy resolution as a function of energy, are summarized. Typical spectroscopy results using a ^{137}Cs radiation source are shown for our crystallites with diameters <1 cm. We obtain energy resolution of 3.2% before packing the crystallite in a sealed detector container and 4.5% after packing. Spectra were also obtained for ^{241}Am, ^{60}Co, ^{228}Th, and background to illustrate the spectrosocopic quality of $CeBr_3$:Ca^{2+} over a broader energy range.

Index Terms—detector, resolution, scintillator materials, gamma ray detector, cerium tribromide; $CeBr_3$; high-resolution detector; halides; rare-earth compounds; scintillator; gamma spectral comparison; resolution; aliovalent substitution

1. INTRODUCTION

The scintillation properties of $CeBr_3$ crystals grown with the divalent dopant Ca^{2+} are presented. Small diameter (up to ~1 cm) single crystals of $CeBr_3$ doped with Ca^{2+} have been grown at Dynasil Radiation Monitoring Devices, Inc. (RMD). The aliovalently calcium-doped cerium tribromide ($CeBr_3$:Ca^{2+}) crystals were prepared according to careful theoretical modeling and delivered to the Remote Sensing Laboratory (RSL) for assessment and evaluation (Fig. 1). $CeBr_3$:Ca^{2+} has a hexagonal crystal structure identical to uranium trichloride (UCl_3). Hexagonal crystals may fracture easily; therefore, their manufacturing yield is expected to be low, making the reliability of large crystals questionable.[1,2] Significant gains in the practical scale for $CeBr_3$ scintillators may be realized by increasing fracture toughness of the crystals.[3] Aliovalent substitution, in which a host ion is replaced with an ion of different valence (e.g., Ca^{2+} for Ce^{3+} in $CeBr_3$) is a more potent method of strengthening than isovalent substitution (i.e., replacing a fraction of ions with like-valence ions). In this approach, the formation of intrinsic defects necessary to maintain charge neutrality results in complexes with long-

* gusspp@nv.doe.gov; phone 1 702 295-8095; fax 1 702 295-8648; nstec.com

range interactions in the crystal. The resulting increase in hardening rate can be explained in terms of elastic interaction with dislocations.[4]

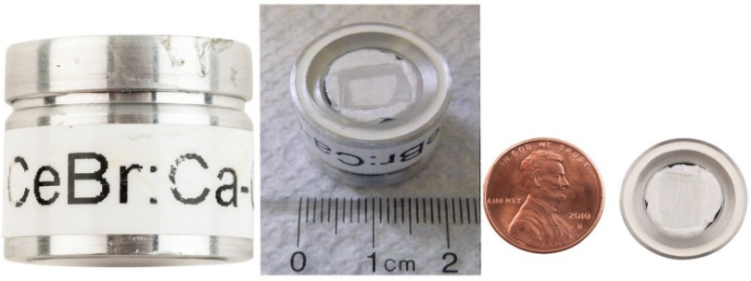

Fig. 1. Packaged scintillator of 0.2 atomic% Ca^{2+}-doped $CeBr_3$.

Because $CeBr_3$ already exhibits superior scintillation characteristics,[5,6] the alloying element(s) used to strengthen the crystal must not degrade the scintillation properties. Aliovalent alloying provides more strengthening than isovalent alloying. The solid solution strengthening τ based on lattice distortions due to some small concentration of dopant can be approximated as

$$\tau = \gamma \bullet Gc^{½}, \tag{1}$$

where G is the shear modulus, c is the concentration of solute in atomic fraction, and γ is a proportionality constant.[7,8] For spherically symmetric distortions, such as those found in isovalent alloying, γ typically takes on values that are significantly smaller than unity, approximately 10^{-4} to 10^{-6}. For tetragonal lattice distortions, such as those created from solute atoms of a different valence, γ can be nearly unity. Therefore, aliovalent alloying is more effective for a given concentration of solute.[8]

2. EXPERIMENTAL DESCRIPTION

A calcium-doped $CeBr_3$:Ca^{2+} crystallite was grown and packaged by RMD. Sandia National Laboratories (SNL) performed density functional theory (DFT) model calculations for a nominal doping (i.e., 2%) of calcium in $CeBr_3$. This helped determine which doping concentrations would lead to changes in optical and mechanical properties. RMD assessed crystal growth strategies for performing growth with lower concentrations of calcium. SNL measured the calcium concentration by the inductively coupled plasma mass spectrometry.

RSL characterized the RMD crystal. RSL acquired spectra with different isotopes using the RMD crystal and the techniques described by Guss.[3,9] The emission spectrum for this crystallite is shown in Fig. 2. These results are consistent with recent findings.[10] The increase in doping level led to a slight blue shift in the emission spectrum. Fig. 3 shows a light output measurement for the crystallite estimated at 62,000 photons per MeV based on comparison to the thallium-doped sodium iodide (NaI:Tl) light yield.

Proportionality of light yield is one area of performance where Ce-doped and Ce-based lanthanide halides excel. Maintaining proportionality is important for producing a strong, high-performance scintillator. Relative light yield proportionality was measured for both doped and undoped samples of $CeBr_3$ to ensure no loss in performance was incurred by aliovalently doping the crystal. The light output and proportionality, however, appear to be similar to that of $CeBr_3$. There was a reduced yield at low energy. Relative light yield proportionality measurements suggest that dopants do not significantly affect proportionality at higher energies. A plot of light yield proportionality for a doped sample is shown in Fig. 4.

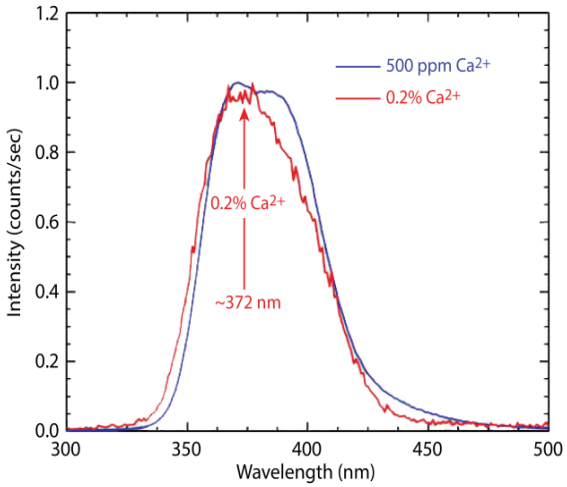

Fig. 2. Emission spectrum measured with 6 × 2 mm 0.2 atomic% Ca^{2+}-doped $CeBr_3$ crystal in the permanent canister compared to a similar measurement for a 500 ppm Ca^{2+}-doped $CeBr_3$ crystal.

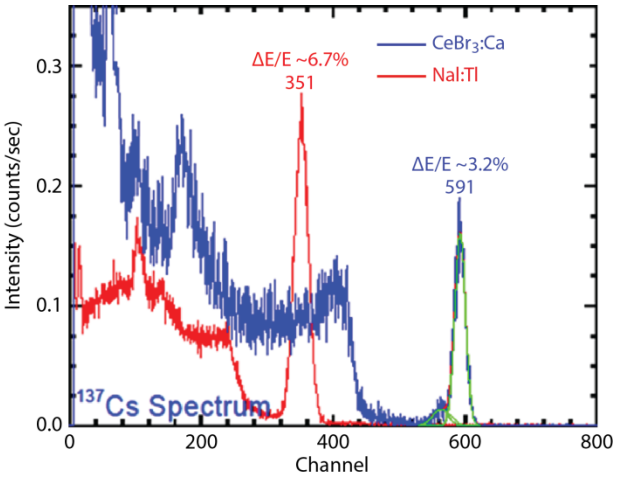

Fig. 3. Light output measurement relative to NaI:Tl indicates 62,000 photons per MeV for Ca^{2+}-doped $CeBr_3$ crystal.

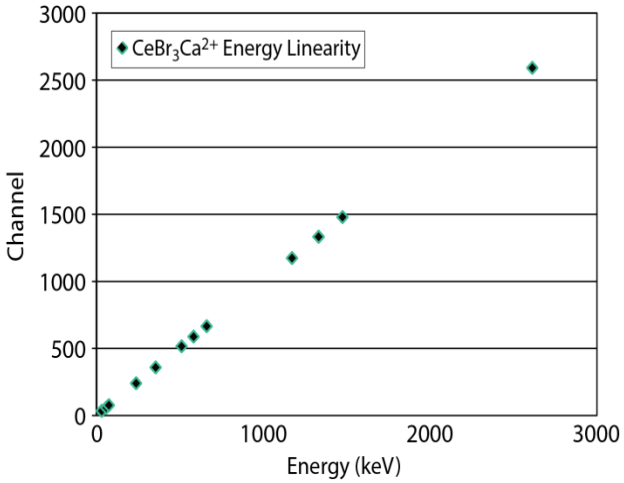

Fig. 4. Relative light yield proportionality of 0.2 atomic% Ca^{2+}-doped $CeBr_3$.

RSL completed additional testing and evaluation of the new crystal as well as the assessment of benchmarking spectroscopy data. Results are well summarized in Fig. 4, which present energy resolution as a function of energy. Typical spectroscopy results using a ^{137}Cs radiation source, including Gaussian fits to the data, are shown in Fig. 5 for our crystallites. We obtain 4.5% for the packaged crystallite. More spectra were obtained for ^{241}Am, ^{60}Co, ^{228}Th, and background to exemplify $CeBr_3$:Ca^{2+} over a broader energy range. The radiation source spectra were acquired for 3600 seconds with the radiation source in contact with the crystal face using typical source strengths of several μCi. The laboratory background acquisition time was 3×10^5 seconds. It was apparent that the packaging of the crystallite impacted the performance of $CeBr_3$:Ca^{2+}. Gaussian fits were made to all the spectral data, as shown in Fig. 5.

We have observed Ca^{2+} to be a most promising dopant, because it significantly reduces the nonproportionality and improves the energy resolution of pure $CeBr_3$. The nonproportionality was measured in the energy range from 32 keV up to 1274 keV. It has been observed that at 32 keV $CeBr_3$:Ca^{2+} deviates about 4% from the ideal case (10% for pure $CeBr_3$). We achieved an excellent energy resolution of 3.2% at 662 keV and light output of ~62,000 photons/MeV.[11,12]

We sought to achieve ultralow activity and high-strength cerium bromide scintillators through a program of refining and alloying with aliovalent strengthening agents (substituents with a different valence than the host lattice). $CeBr_3$ is a self-activated lanthanide scintillator that has received considerable recent attention[13] due to its proportionality and energy resolution for gamma spectroscopy being far superior to that of NaI:Tl. Because the material possesses no intrinsic radioactivity, $CeBr_3$ has a high potential to outperform scintillators such as cerium-activated lanthanum tribromide or lanthanum-based elpasolites,[14] making it an excellent candidate for gamma spectrometers for passive detection and identification of special nuclear material.[15,16] However, due to its hexagonal crystal structure (UCl_3), pure $CeBr_3$ can fracture during crystal growth, detector fabrication, and subsequent use under field conditions, thus impacting manufacturing yield and reliability for large crystals.[2]

Aliovalent substitution, in which a host ion is replaced with an ion of different valence (e.g., Cd^{2+} for Ce^{3+} in $CeBr_3$) is a more potent method of strengthening than isovalent substitution (i.e., replacing a fraction of ions with like-valence ions). The formation of intrinsic defects necessary to maintain charge neutrality results in complexes with long-range interactions in the crystal. The resulting increase in hardening rate can be explained in terms of elastic interaction (tetragonal distortion) with dislocations.[4] Concentration levels necessary to increase the yield strength by an order of magnitude may be in the 100–500 ppm range (0.01%–0.05%) for aliovalent substitution, whereas isovalent substitution may require 10%–50% to achieve the same effect.

For these reasons, aliovalent substitution was chosen to improve the strength of $CeBr_3$. SNL demonstrated success with this approach, achieving a dramatic reduction of fracture in aliovalent alloys compared with pure $CeBr_3$ crystals.[8] Prototype ingots were compounded with the addition of 2% of $CaBr_2$ added to a high-purity $CeBr_3$ charge in a closed ampoule before melting and solidification in a gradient-freeze process. Pure $CeBr_3$ ingots solidified under these conditions were severely fractured, yielding only centimeter-sized shards. The lesson learned was that 2% was too high of a charge for the calcium. Therefore, we needed to perform mass analysis of the material and recalculate the DFT with a lower charge of calcium. We also performed an assessment of the spectroscopic performance of the $CeBr_3$:Ca shards delivered by RMD to RSL.

The 2% calcium-doped $CeBr_3$:Ca crystallite was grown and packaged by RMD. Several minor tasks remained to complete characterization of the calcium-doped crystal. SNL performed DFT model calculations with less dilute doping (i.e., something less than 2%) of calcium in $CeBr_3$. This helped assess what doping concentration would lead to changes in optical and mechanical properties. RMD assessed crystal growth strategies for performing growth with lower concentrations of calcium. RSL assessed the spectroscopic performance of the crystal. RSL acquired spectra with different isotopes using the RMD crystal using the techniques described by Guss.[3,17,18] The emission spectrum for this crystallite is shown in Fig. 2. Fig. 3 shows a light output measurement for the crystallite estimated at 62,000 photons per MeV based on comparison to the NaI:Tl light yield.

Figs. 3 and 6 present a comparison of the ^{137}Cs radiation source spectra and proportionality before and after packaging and sealing into the hermetically sealed canister sent to RSL. A slight degradation in performance is associated with the permanent package of the crystal. Fig. 6 also illustrates the improvement in linearity achieved by doping the $CeBr_3$ with Ca^{2+}. The spectra shown in Fig. 6 were also fit to a Gaussian shape, with low-energy tail, to obtain the indicated spectra energy resolutions.

3. CALCIUM CONCENTRATION

We have measured the calcium concentration in the $CeBr_3$ by the inductively coupled plasma mass spectrometry (ICP-MS) technique from the crystals prepared by RMD. ICP-MS is a type of mass spectrometry capable of detecting metals and several non-metals at concentrations as low as one part in 10^{12} (part per trillion). SNL performed the ICP-MS. SNL also calculated a DFT model with less dilute doping (i.e., something less than 2%) of calcium in $CeBr_3$. SNL analyzed the concentration of calcium in the crystals. Referring to Table 1, we used the average calcium weight % concentration, $x = 0.000214$, in our complex of $Ce_{(1-x)}Ca_xBr_{(3-x)}$, to evaluate the formula for atomic percentage:

$$\text{Atomic \%} = 40.078x/[140.116\,(1 - x) + 40.078x + 79.904\,(3 - x)] = 0.00228 = 0.228\% \,. \quad (2)$$

Based on our measurements, using three different samples (~0.2 grams), we have three consistent data sets indicating that the calcium concentration in these crystals is 0.0214 ±0.0102 wt.% (one σ) by weight, which corresponds to an atom percentage of 0.228 atomic%. This value seems to be much less than the batch formulation. We do not know if there is a solubility limit or a composition gradient in the ingot (sampling). Our data will be used to extract the solubility limit.

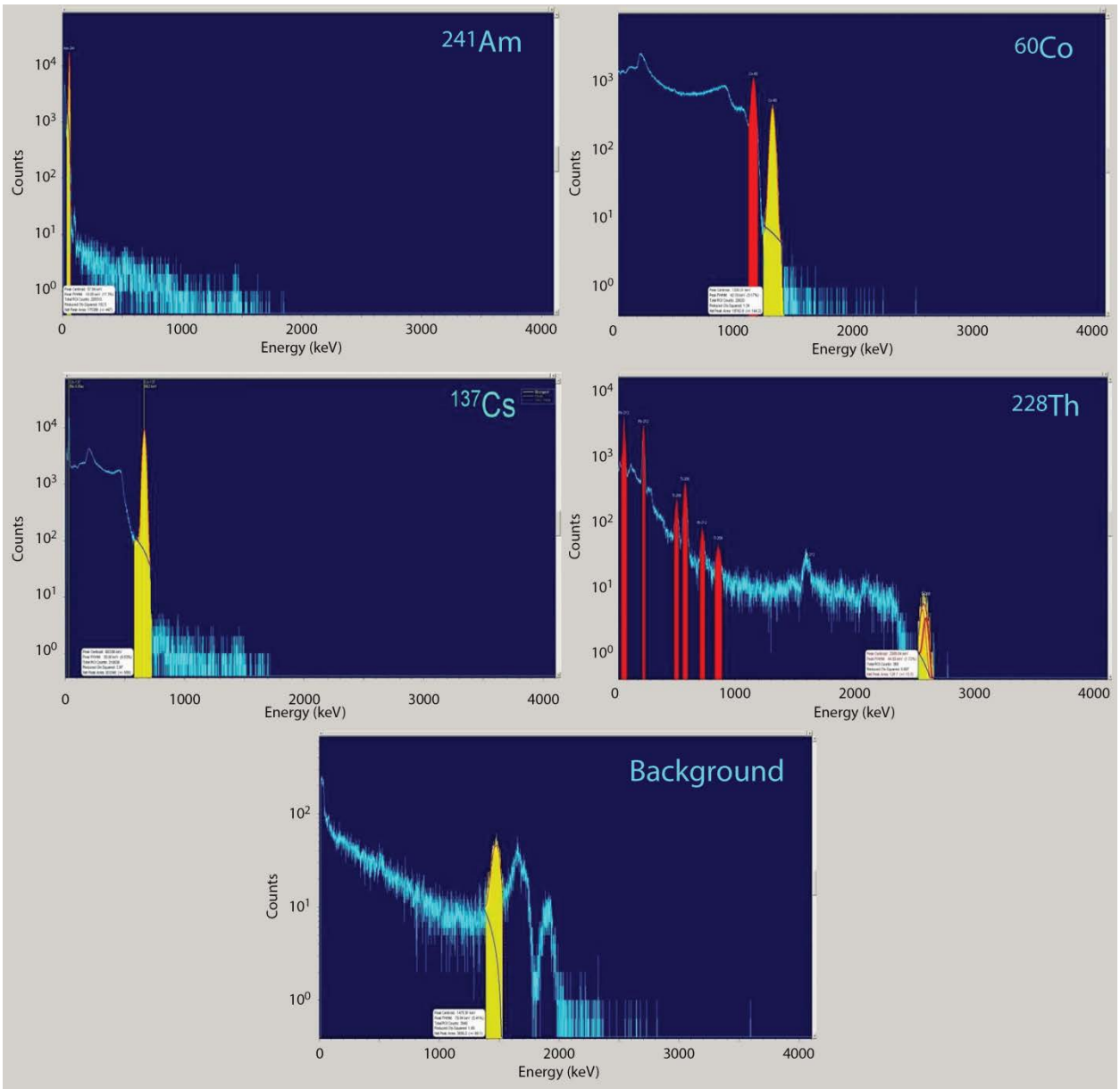

Fig. 5. ^{241}Am, ^{60}Co, ^{137}Cs, ^{228}Th, and background spectra with 0.228 at % Ca^{2+}-doped $CeBr_3$ in the permanent canister. Plots show fits superimposed on data.

The objective of this portion of the task was to experimentally determine the solubility of $CaBr_2$ in the intrinsic scintillator $CeBr_3$. Our initial approach attempted equilibrium solid-state diffusion at several elevated temperatures for various amounts of time to allow Ca^{2+} to diffuse into the cerium bromide lattice, followed by chemical analysis to

determine solubility limit and the activation energy for diffusion. However, this approach resulted in partial melting/fusion of the samples; therefore, a set of differential scanning calorimetric (DSC) measurements were performed and combined with our existing segregation data from crystal growth to build a working phase diagram in the $CeBr_3$-rich region.

The chemical analysis of three $CeBr_3$ samples from a nominal 2% ingot grown by RMD is summarized in Table 1. The ICP-MS was used to determine as-grown concentrations of calcium with approximately 5% precision. Assuming the growth conditions were near equilibrium, an estimate for the segregation coefficient K_{eff} is $C_S/C_L = 0.11$. Therefore, the slope of the solidus line near 2% $CaBr_2$ in the liquid can be estimated by establishing a liquidus line from melting point data.

Table 2 is a tabulation of DSC data taken on samples in the composition range of 0%–10% $CaBr_2$ by mole. While the measured melting temperature T_m for the pure $CeBr_3$ sample appears anomalous and is in poor agreement with the literature, the mixtures show linear trends, including an apparent eutectic temperature T_e near 597ºC for calcium concentrations ≥2.35%.

Table 1. ICP-MS assays for Ca(II)-doped $CeBr_3$; nominal composition 2 wt% $CaBr_2$ in $CeBr_3$

Sample	Calcium Concentration	95% Confidence Limit
#1	0.0238 wt%	0.0014 wt%
#2	0.0212 wt%	0.0015 wt%
#3	0.0192 wt%	0.0015 wt%

Table 2. DSC results for $CeBr_3$-$CaBr_2$ mixtures in the range 0–10 mole %

Mole % $CaBr_2$	Tm	Te
0	715.3ºC	–
0.2	732.1ºC	–
2.35	721.8ºC	598.3ºC
4.65	715.2ºC	595.4ºC
7.63	706.8ºC	596.2ºC
9.85	697.3ºC	597.0ºC

All results are plotted in Fig. 7, on which approximate solidus, liquidus, and eutectic lines have been constructed. Not plotted are some additional data taken at 20% and 30%, which indicate the liquidus continues the near-linear trend. Note that our current experimental upper bound for the solid solubility is the data point at 2.35%, which must lie well within the α + β field, since the eutectic temperature T_e was detected. This concentration is considerably less than the intersection of the extrapolated solidus and the eutectic temperature; therefore, the solidus line is clearly nonlinear and probably exhibits retrograde solubility well below the melting point of pure $CeBr_3$, as is commonly observed for sparingly soluble impurities in other systems. This behavior can be characterized as a variation of the segregation coefficient with temperature, as analyzed by Hall.[19] For example, the maximum solid solubility for sparingly soluble impurities in silicon and germanium follow a simple empirical correlation with k_0, the limiting equilibrium segregation coefficient, as C_L approaches 0: $C_{S,max} = k_0/10$.[20] Based on this relation, the solidus was arbitrarily extrapolated to $k_{eff}/10 = 1.1\%$ at the eutectic temperature to estimate the minimum extent of the eutectic line towards the $CeBr_3$ side of the phase diagram (Fig. 7).

It should be noted that the eutectic composition extrapolated from the points plotted is near 37% calcium; however, the nominal 20% and 30% data indicate it could be near 50%. More experiments are needed to accurately determine both the eutectic composition and the β phase, which could reasonably be expected to be a ternary such as $CaCeBr_5$ or Ca_2CeBr_7.

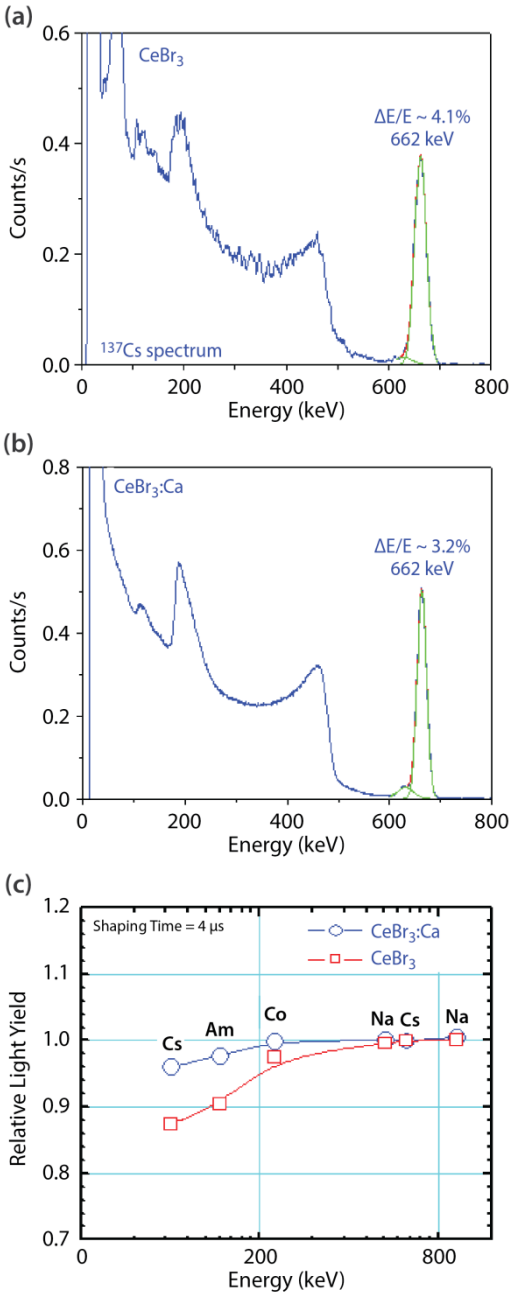

Fig. 6. (a) 662 keV spectrum with standard $CeBr_3$ with ~4% FWHM, (b) 662 keV spectrum with $CeBr_3$:Ca^{2+} with ~3.2% FWHM, (c) plots showing improved proportionality for $CeBr_3$:Ca^{2+} over standard $CeBr_3$. Plots show fits superimposed on data.

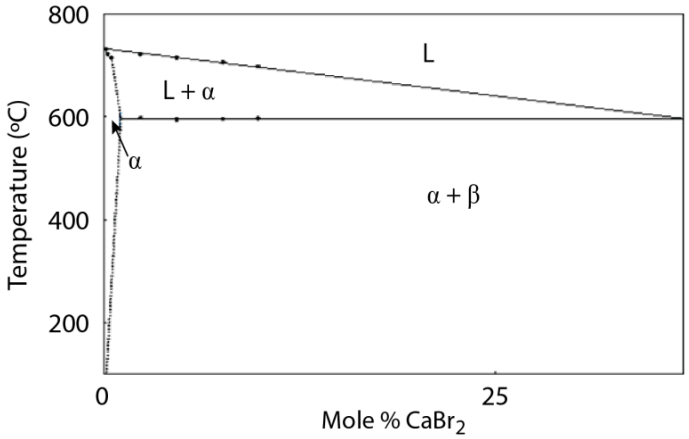

Fig. 7. Phase diagram for $CeBr_3$-$CaBr_2$.

4. RESULTS AND DISCUSSION

SNL performed microhardness measurements to see if the aliovalent approach hardened the crystal as expected. Microhardness (Vickers hardness[21]) and indentation toughness of these samples were measured. Due to the size limitation, we could not obtain sufficient statistics and confidence on these measured values. Therefore, we do not report the results here. Future work should include studies in correlation between sheer strength and Ca^{2+} concentration.

Based on the recent literature on strengthening mechanisms,[22] there are compelling requirements to research and several ideas, questions, and answers to share. Sinha's paper on aliovalent strengthening of CaF_2 attempts to determine mechanisms for low and high temperatures. Sinha and Nicholson[22] found that Y(III) gave an order of magnitude greater increase in critical resolve shear stress than Na(I). They conclude the long-range retarding force on dislocations at high temperature is likely due to the induced reorientation of Na(I)/F-vacancy or Y(III)/F-interstitial dipoles in the stress fields of moving dislocations (Snoek effect). This suggested role of the Snoek effect[23] is in accord with analysis of the athermal regime in recent papers on Y stabilized zirconia and other materials.[5,13,24–30] If the authors are correct that anion interstitials balance the charge for the higher valence cation, then the difference in strength may be related to the higher mobility of interstitials. The interstitial fluoride ion in CaF_2 may be more plausible than interstitial bromide; however, the $CeBr_3$ crystal structure does have large open channels. We examined whether the M(IV)/Br-interstitial seems like a feasible complex in $CeBr_3$. Because the athermal (high-temperature) regime is probably more important during crystal growth, future work should explore if it makes sense to place more emphasis on M(IV) cations silicon, tin, lead, titanium, zirconium, hafnium, rhenium, molybdenum, cerium, thorium, protactinium, uranium, neptunium, and plutonium.

5. SUMMARY

To summarize, new DFT simulations demonstrate a capability for predicting properties of doped $CeBr_3$ materials that is unavailable elsewhere but is critically needed to study the property-limiting valence phenomena in ionic compounds. During this project, we assessed concentrations and the solubility limit. RSL benchmarked the Ca^{2+}-doped $CeBr_3$ crystal. The Ca^{2+}-doped $CeBr_3$ crystal has improved energy resolution (i.e., 3.2%) and linearity over the pure $CeBr_3$ crystal.

ACKNOWLEDGMENTS

Marlene Bencomo (University of New Mexico, Albuquerque) assisted with ICP-MS analysis. The authors acknowledge the professional staff of RMD, Watertown, Massachusetts, for the production of the detectors, for providing these

detectors to the Remote Sensing Laboratory, and for their support and advice. The authors thank Michael Lukens, John O'Donoghue, and Michael Reed for their contributions.

This manuscript has been authored by National Security Technologies, LLC, under Contract No. DE-AC52-06NA25946 with the U.S. Department of Energy and supported by the Site-Directed Research and Development Program. The United States Government retains and the publisher, by accepting the article for publication, acknowledges that the United States Government retains a non-exclusive, paid-up, irrevocable, world-wide license to publish or reproduce the published form of this manuscript, or allow others to do so, for United States Government purposes. The U.S. Department of Energy will provide public access to these results of federally sponsored research in accordance with the DOE Public Access Plan (http://energy.gov/downloads/doe-public-access-plan).

REFERENCES

[1] Doty, F. P., McGregor, D., Harrison, M., Findley, K., and Polichar, R., "Structure and properties of lanthanide halides," Proc. SPIE 6707, 670705:1-11 (2007).

[2] Doty, F. P., McGregor, D., Harrison, M., Findley, K., Polichar, R., and Yang, P., "Basic materials studies of lanthanide halide scintillators," MRS Proc. 1038, 1-8 (2008).

[3] Guss, P., Wong, B., Foster, M., Doty, F. P., Shah, K., Squillante, M., Glodo, J., and Yuan, D., "Low-cost cerium bromide alloys," Site-Directed Research and Development, FY 2012, National Security Technologies, LLC, Las Vegas, Nevada, 11-19 (2013).

[4] Pletka, B. J., Mitchell, T. E., and Heuer, A. H., "Solid solution hardening of sapphire (α-Al_2O_3)," Physica Status Solidi (a) 39(1), 301-311 (1977).

[5] Shah, K. S., Glodo, J., Higgins, W., van Loef, E., Moses, W. W., Derenzo, S. E., and Weber, M. J., "$CeBr_3$ scintillators for gamma-ray spectroscopy," IEEE Trans. Nucl. Sci. 52(6), 3157-3159 (2005).

[6] Ra, S., Kim, S., Kim, H. J., Park, H., Lee, S., Kang, H., and Doh, S.-H., "Luminescence and scintillation properties of a $CeBr_3$ single crystal," IEEE Trans. Nucl. Sci. 55(3), 1221-1224 (June 2008).

[7] Courtney, T. H., Mechanical Behavior of Materials, 2nd edition, Waveland, Long Grove, Illinois, 232 (2000).

[8] Harrison, M. J., Ugorowski, P., Linnick, C., Brinton, S., McGregor, D. S., Doty, F. P., Kirpatrick, S., and Bahr, D. F., "Aliovalent doping of $CeBr_3$," Proc. SPIE 7806, 78060M-1-78060M-14 (2010).

[9] Guss, P. P., Guise, R. Mitchell, S., Mukhopadhyay, S., Lowe, D., O'Brien, R., and Yuan, D., "Nanostructured lanthanum halides and $CeBr_3$ for nuclear radiation detection," Site-Directed Research and Development, FY 2010, National Security Technologies, LLC, Las Vegas, Nevada, 55-64 (2010).

[10] Quarati, F. G. A., Dorenbos, P., van der Biezen, J., Owens, A., Selle, M., Parthier, L., and Schotanus, P., "Scintillation and detection characteristics of high-sensitivity $CeBr_3$ gamma-ray spectrometers," Nucl. Instrum. Methods Phys. Res. A 729, 596-604 (2010). http://dx.doi.org/10.1016/j. nima.2013.08.005.

[11] Guss, P., Stampahar, T., Foster, M. E., Wong, B. M., Doty, P., Yang, P., Shah, K., Squillante, M., Shirwadkar, U., Hawrami, R., Tower, J., Mukhopadhyay, S., and Yuan, D., "Low-cost cerium bromide alloys," Site-Directed Research and Development, FY 2013, National Security Technologies, LLC, Las Vegas, Nevada, 221-234 (2010).

[12] Shirwadkar, U., Hawrami, R., van Loef, E., Tower, J., Squillante, M., Shah, K., Guss, P., Stampahar, T., Foster, M., Wong, B., Doty, F. P., and Yuan, D., "Scintillation properties of $CeBr_3$ with divalent doping," Proceedings of the 20th Conference on Room-Temperature Semiconductor X- and Gamma-Ray Detectors, (RTSD Conference), IEEE 2013 Nuclear Science Symposium and Medical Imaging Conference, Scintillator Properties. COEX Convention Center, Seoul, South Korea, N-4, October 27-November 1 (2013).

[13] Shah, K. S., Glodo, J., Higgins, W., van Loef, E., Moses, W. W., Derenzo, S. E., and Weber, M. J., "$CeBr_3$ scintillators for gamma-ray spectroscopy," IEEE Trans. Nucl. Sci. 52(6) 3157-3159 (2005).

[14] Guss, P. P., Reed, M., Yuan, D., Reed, A., and Mukhopadhyay, S., "$CeBr_3$ as a room-temperature, high-resolution gamma-ray detector," Nucl. Instrum. Methods Phys. Res. A 608(2), 297-304 (2009).

[15] Shah, K. S., Glodo, J., Klugerman, M., Higgins, W. M., Gupta, T., and Wong, P., "High energy resolution scintillation spectrometers," IEEE Trans. Nucl. Sci. 51(5), 2395-2399 (2004).

[16] Guss, P., Reed, M., Yuan, D., Cutler, M., Contreras, C., and Beller, D., "Comparison of CeBr3 with LaBr3:Ce, LaCl3:Ce, and NaI:Tl detectors," Proc. SPIE 7805, L-1 (2010).

[17] Guss, P., Foster, M. E., Wong, B. M., Doty, F. P., Shah, K., Squillante, M., Shirwadkar, U., Hawrami, R. Tower, J., Yuan, D., "Linearity for Ca^{2+}-Doped $CeBr_3$ Scintillating Materials," 2014 Symposium on Radiation

Measurements and Applications (SORMA XV) Ann Arbor, MI; June 9-13 (2014) 022. http://rma-symposium.engin.umich.edu/program.php, accessed January 9, 2015.

[18] Guss, P., Foster, M. E., Wong, B. M., Doty, F. P., Shah, K., Squillante, M. R., Shirwadkar, U., Hawrami, R., Tower, J. and Yuan. D., "Results for aliovalent doping of $CeBr_3$ with Ca^{2+}," J Appl. Phys. 115(3), 034908-1 (17 January 2014).

[19] Hall, R. N., "Variation of the distribution coefficient and solid solubility with temperature," J. Phys. Chem. Solids 3(1-2), 63-73 (1957).

[20] Fischler, S., "Correlation between maximum solid solubility and distribution coefficient for impurities in Ge and Si," J. Appl. Phys. 33(4), 1615 (1962).

[21] Smith, R. L. and Sandland, G. E., "An accurate method of determining the hardness of metals, with particular reference to those of a high degree of hardness," Proceedings of the Institution of Mechanical Engineers, I 623-641 (1922).

[22] Sinha, M. N. and Nicholson, P. S., "Effect of impurities on the strengthening of CaF_2 single crystals," J. Mat. Sci. 12(7), 1451-1462 (1977).

[23] Snoek, J. L., "Effect of small quantities of carbon and nitrogen on the elastic and plastic properties of iron," Physica 8(7), 711-733 (1941).

[24] Baither, D., Baufeld, B., Messerschmidt, U., and Bartsch, M., "HVEM high-temperature in situ straining experiments on cubic zirconia single crystals," Materials Science and Engineering A 233, 75-87 (1997).

[25] Lassila, D. H., Goldberg, A., and Becker, R., "The effect of grain boundaries on the athermal stress of tantalum and tantalum-tungsten alloys," Metallurgical and Materials Transactions A 33(11), 3457-3464 (November 2002).

[26] Mercer, C., Williams, J. R., Clarke, D. R., and Evans, A. G., "On a ferroelastic mechanism governing the toughness of metastable tetragonal-prime (*t'*) yttraia-stabilized zirconia," Proc. R. Soc. A 463(2081), 1393-1408 (8 May 2007) http://www.materials.ucsb.edu/MURI/ papers/Merceretal_PRS07.pdf, accessed December 12, 2013.

[27] Armengol, S., "Caracterización Microestructural de un recubrimiento de YSZ para aplicaciones biomédicas," IV. Latin American Congress on Biomedical Engineering 2007, Bioengineering Solutions for Latin America Health, IFMBE Proceedings 18, 671-675 (8 May 2007).

[28] Martin, H. and Pippan, R., "Athermal and thermal limits of the grain refinement by SPD," Materials Science Forum, Trans Tech Publications, Switzerland 584-586, 938-943 (2008).

[29] Taherabadi, L., Trujillo, J. E., Chen, T., Porter, J. R., and Mecartney, M. L., "Observation of dislocation assisted high temperature deformation in mullite and mullite composites," J. European Ceramic Soc. 28(2), 371-376 (2008).

[30] Gan, Y. X., Pothula, S. V., and Franchetti, M. J., "Plasticity of nanoporous Ni/YSZ anode: A numerical analysis," ASME 2010 8th International Conference on Fuel Cell Science, Engineering and Technology, Brooklyn, New York, USA, June 14-16, 2010, 153-158 (2010).